Fractional dynamics in the trajectory control of redundant manipulators

Maria da Graça Marcos [a], Fernando B.M. Duarte [c,*], J.A. Tenreiro Machado [b]

Abstract

Under the pseudoinverse control, robots with kinematical redundancy exhibit an undesirable chaotic joint motion which leads to an erratic behavior. This paper studies the complexity of fractional dynamics of the chaotic response. Fourier and wavelet analysis provides a deeper insight, helpful to know better the lack of repeatability problem of redundant manipulators. This perspective for the study of the chaotic phenomena will permit the development of superior trajectory control algorithms.

Keywords: Redundant manipulators; Fractional calculus; Fourier transform; Windowed Fourier transform; Wavelets

1. Introduction

A kinematically redundant manipulator is a robotic arm possessing more degrees of freedom (*dof*) than those required to establish an arbitrary position and orientation of the gripper. Redundant manipulators offer several potential advantages over non-redundant arms. In a workspace with obstacles, the extra degrees of freedom can be used to move around or between obstacles and thereby to manipulate in situations that otherwise would be inaccessible [1–4].

When a manipulator is redundant, it is anticipated that the inverse kinematics admits an infinite number of solutions. This implies that, for a given location of the manipulator's gripper, it is possible to induce a self-motion of the structure without changing the location of the end effecter. Therefore, the arm can be reconfigured to find better postures for an assigned set of task requirements.

Several kinematic techniques for redundant manipulators control the gripper through the rates at which the joints are driven, using the pseudoinverse of the Jacobian [3,6]. Nevertheless, these algorithms lead to a kind of chaotic motion with unpredictable arm configurations.

Having these ideas in mind, the paper is organized as follows. Section 2 introduces the fundamental issues for the kinematics of redundant manipulators. Based on these concepts, Section 3 presents the trajectory control of a three *dof* robot. The results reveal a chaotic behavior that is further analyzed in Section 4. Finally, Section 5 draws the main conclusions.

2. Kinematics of redundant manipulators

A kinematically redundant manipulator is a robotic arm possessing more *dof* than those required to establish an arbitrary position and orientation of the gripper. In Fig. 1 is depicted a planar manipulator with $k \in \aleph$ rotational (R) joints that is redundant for $k > 2$.

When a manipulator is redundant it is anticipated that the inverse kinematics admits an infinite number of solutions. This implies that, for a given location of the manipulator's gripper, it is possible to induce a self-motion of the structure without changing the location of the gripper. Therefore, redundant manipulators can be reconfigured to find better postures for an assigned set of task requirements but, on the other hand, have a more complex structure requiring adequate control algorithms.

We consider a manipulator with n degrees of freedom whose joint variables are denoted by $\mathbf{q} = [q_1, q_2, \ldots, q_n]^{\mathrm{T}}$. We assume that a class of tasks we are interested in can be described by m variables, $\mathbf{x} = [x_1, x_2, \ldots, x_m]^{\mathrm{T}} (m < n)$ and that the relation between $\mathbf{q}$ and $\mathbf{x}$ is given by

$$\mathbf{x} = f(\mathbf{q}), \tag{1}$$

where f is a function representing the direct kinematics. Differentiating (1) with respect to time yields:

$$\dot{\mathbf{x}} = \mathbf{J}(\mathbf{q})\dot{\mathbf{q}}, \tag{2}$$

where $\dot{\mathbf{x}} \in \Re^m, \dot{\mathbf{q}} \in \Re^n$ and $\mathbf{J}(\mathbf{q}) = \partial f(\mathbf{q})/\partial \mathbf{q} \in \Re^{m \times n}$. Hence, it is possible to calculate a path $\mathbf{q}(t)$ in terms of a prescribed trajectory $\mathbf{x}(t)$ in the operational space. We assume that the following condition is satisfied

$$\max \operatorname{rank}\{\mathbf{J}(\mathbf{q})\} = m. \tag{3}$$

Failing to satisfy this condition usually means that the selection of manipulation variables is redundant and the number of these variables m can be reduced. When condition (3) is verified, we say that the degree of redundancy of the manipulator is $n - m$. If, for some $\mathbf{q}$ we have

$$\operatorname{rank}\{\mathbf{J}(\mathbf{q})\} < m, \tag{4}$$

then the manipulator is in a singular state. This state is not desirable because, in this region of the trajectory, the manipulating ability is very limited.

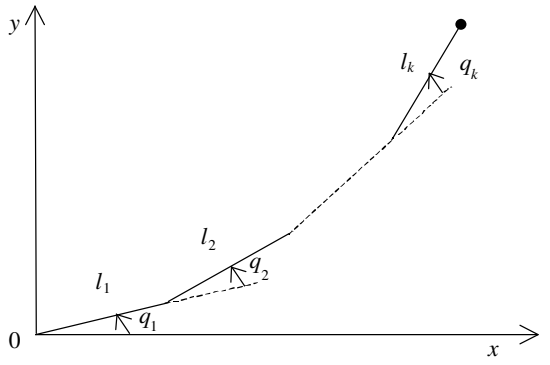

Fig. 1. A planar redundant planar manipulator with k rotational joints.

Many approaches for solving redundancy [5,8] are based on the inversion of Eq. (2). A solution in terms of the joint velocities is sought as

$$\dot{\mathbf{q}} = \mathbf{J}^{\#}(\mathbf{q})\dot{\mathbf{x}}, \tag{5}$$

where $\mathbf{J}^{\#}$ is the Moore-Penrose generalized inverse of the Jacobian [8,9].

It can be easily shown that a more general solution to Eq. (2) is given by:

$$\dot{\mathbf{q}} = \mathbf{J}^{\#}(\mathbf{q})\dot{\mathbf{x}} + [\mathbf{I} - \mathbf{J}^{\#}(\mathbf{q})\mathbf{J}(\mathbf{q})]\dot{\mathbf{q}}_0 \tag{6}$$

where $\mathbf{I}$ is the $n \times n$ identity matrix and $\dot{\mathbf{q}}_0 \in \Re^n$ is a $n \times 1$ arbitrary joint velocity vector and $\mathbf{J}^{\#}$ is the pseudo-inverse of the $\mathbf{J}$. The solution (6) is composed of two terms. The first term is relative to minimum norm joint velocities. The second term, the *homogeneous solution*, attempts to satisfy the additional constraints specified by $\dot{\mathbf{q}}_0$. Moreover, the matrix $\mathbf{I} - \mathbf{J}^{\#}(\mathbf{q})\mathbf{J}(\mathbf{q})$ allows the projection of $\dot{\mathbf{q}}_0$ in the null space of $\mathbf{J}$. A direct consequence is that it is possible to generate internal motions that reconfigure the manipulator structure without changing the gripper position and orientation [7–11]. Another aspect revealed by the solution of (5) is that repetitive trajectories in the operational space do not lead to periodic trajectories in the joint space. This is

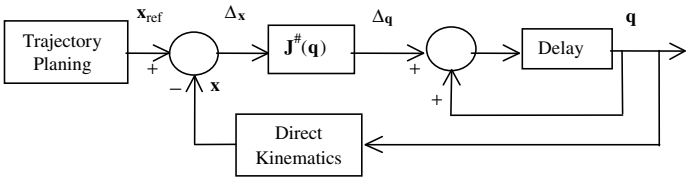

Fig. 2. Block diagram of the closed-loop inverse kinematics algorithm with the pseudoinverse.

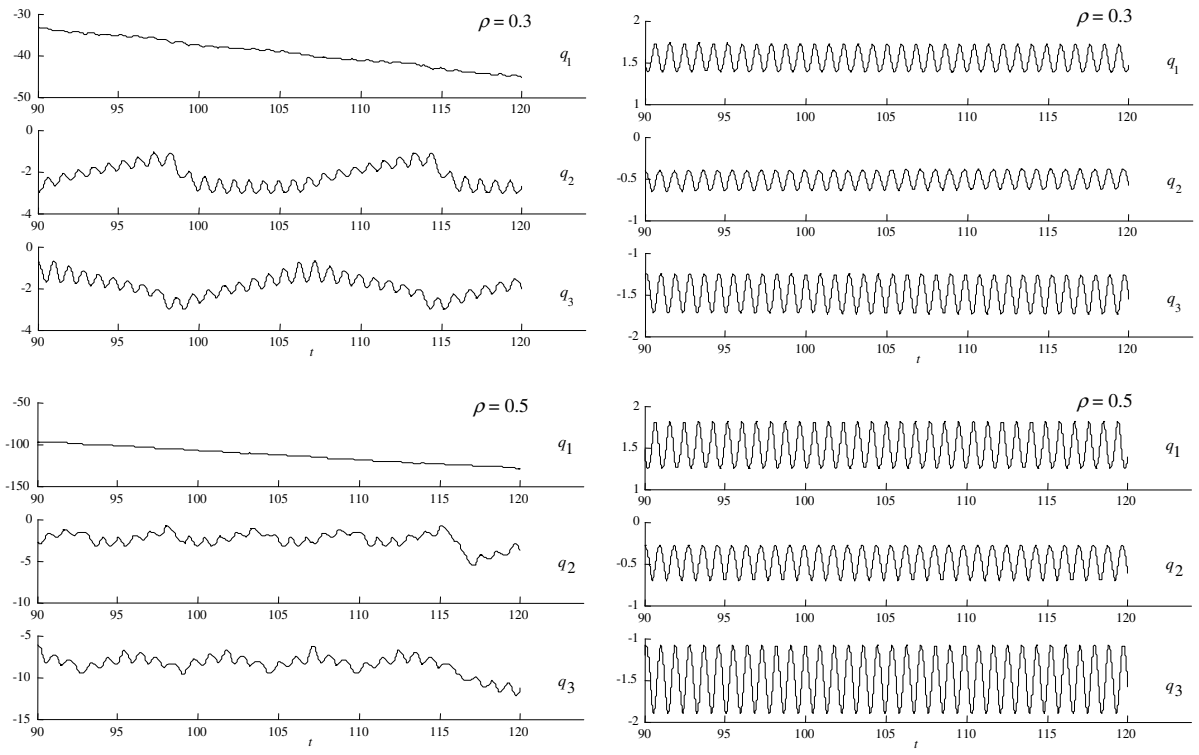

Fig. 3. The 3*R*-robot joint positions versus time using the pseudoinverse method for $r = \{0.6, 2.0\}$ and $\rho = \{0.3, 0.5\}$.

an obstacle for the solution of many tasks because the resultant robot configurations have similarities with those of a chaotic system.

3. Robot trajectory control

The direct kinematics and the Jacobian of a 3-link planar manipulator with rotational joints (3R robot) has a simple recursive nature according with the expressions:

$$\begin{bmatrix} x \\ y \end{bmatrix} = \begin{bmatrix} l_1C_1 + l_2C_{12} + l_3C_{123} \\ l_1S_1 + l_2S_{12} + l_3S_{123} \end{bmatrix} \tag{7.a}$$

$$\mathbf{J} = \begin{bmatrix} -l_1S_1 - \cdots - l_3S_{123} & \cdots & -l_3S_{123} \\ l_1C_1 + \cdots + l_3C_{123} & \cdots & l_3C_{123} \end{bmatrix} \tag{7.b}$$

where l_i is the length of link $i, q_{i\ldots k} = q_i + \cdots + q_k, S_{i\ldots k} = \sin(q_{i\ldots k})$ and $C_{i\ldots k} = \cos(q_{i\ldots k})$.

During all the experiments it is considered $\Delta t = 10^{-3}$ sec, $L_{\mathrm{TOT}} = l_1 + l_2 + l_3 = 3$ and $l_1 = l_2 = l_3$.

In the closed-loop pseudoinverse's method the joint positions can be computed through the time integration of the velocities according with the block diagram of the inverse kinematics algorithm depicted in Fig. 2 where $\mathbf{x}_{\mathrm{ref}}$ represents the vector of reference coordinates of the robot gripper in the operational space.

Based on Eq. (7) we analyze the kinematic performances of the 3R-robot when repeating a circular motion in the operational space with frequency $\omega_0 = 7.0$ rad sec^{-1}, centre at distance $r = [x^2 + y^2]^{1/2}$ and radius ρ.

Fig. 3 show the joint positions for the inverse kinematic algorithm (5) for $r = \{0.6, 2.0\}$ and $\rho = \{0.3, 0.5\}$.

We observe that

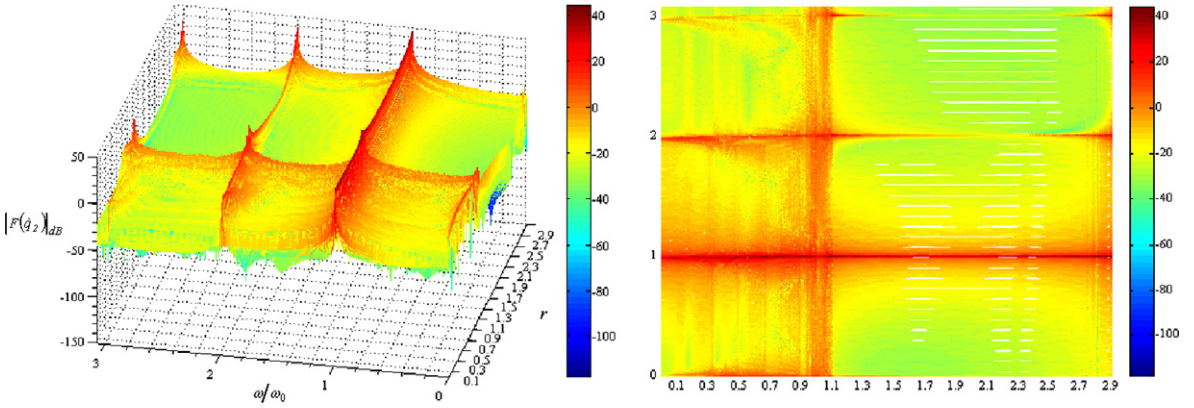

Fig. 4. $|F\{\dot{q}_2(t)\}|$ of the 3R-robot during 300 cycles, versus r and ω/ω_0, for $\rho = 0.1$, $\omega_0 = 7.0$ rad sec^{-1}.

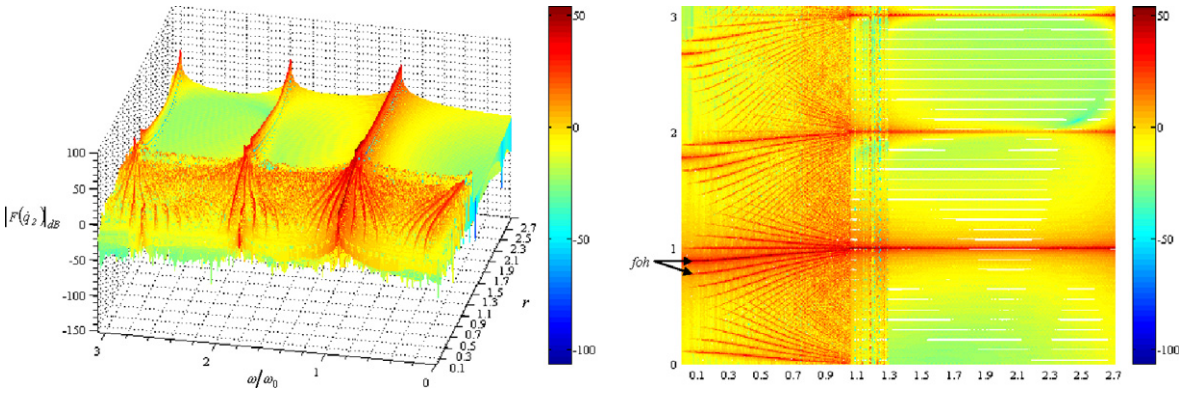

Fig. 5. $|F\{\dot{q}_2(t)\}|$ of the 3R-robot during 300 cycles, versus r and ω/ω_0, for $\rho = 0.3$, $\omega_0 = 7.0$ rad sec^{-1}.

– For $r = 0.6$ occur unpredictable motions with severe variations that lead to high joint transients [12]. Moreover, we verify a low frequency signal modulation that depends on the circle being executed.
– For $r = 2.0$ the motion is periodic with frequency identical to $\omega_0 = 7.0$ rad sec^{-1}.

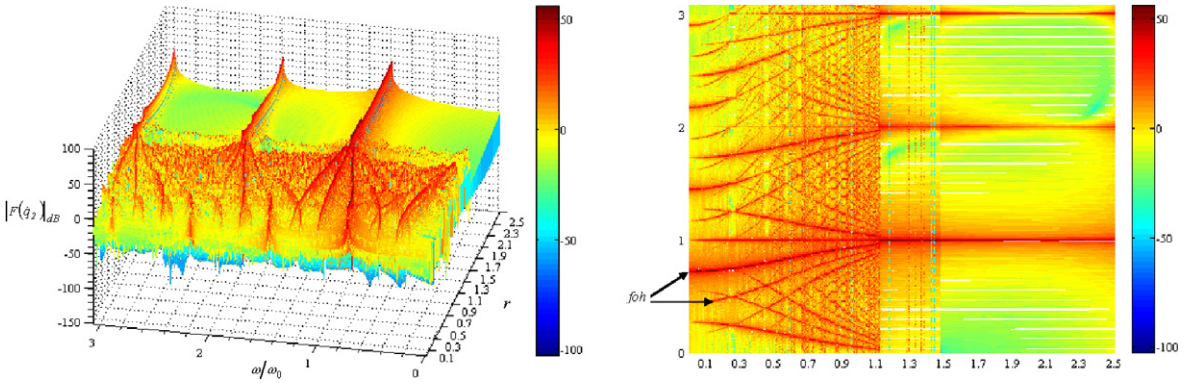

Fig. 6. $|F\{\dot{q}_2(t)\}|$ of the 3R-robot during 300 cycles, versus r and ω/ω_0, for $\rho = 0.5$, $\omega_0 = 7.0$ rad sec^{-1}.

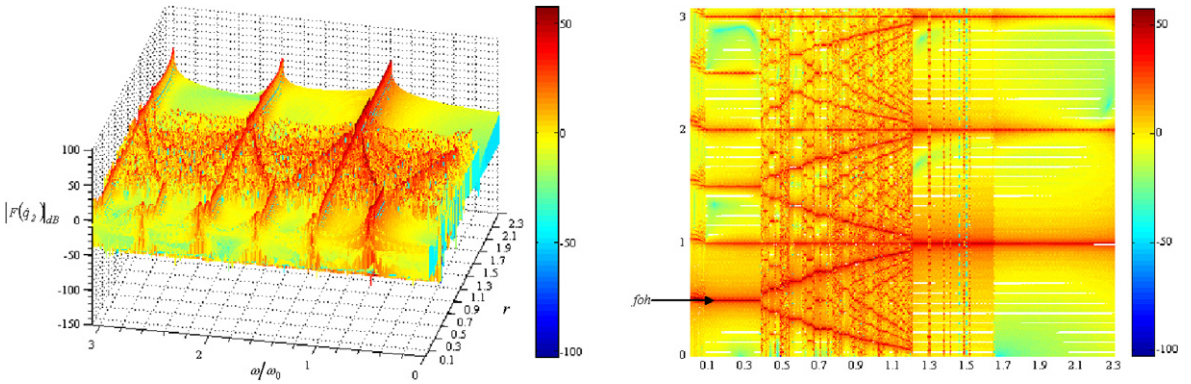

Fig. 7. $|F\{\dot{q}_2(t)\}|$ of the 3R-robot during 300 cycles, versus r and ω/ω_0, for $\rho = 0.7$, $\omega_0 = 7.0$ rad sec^{-1}.

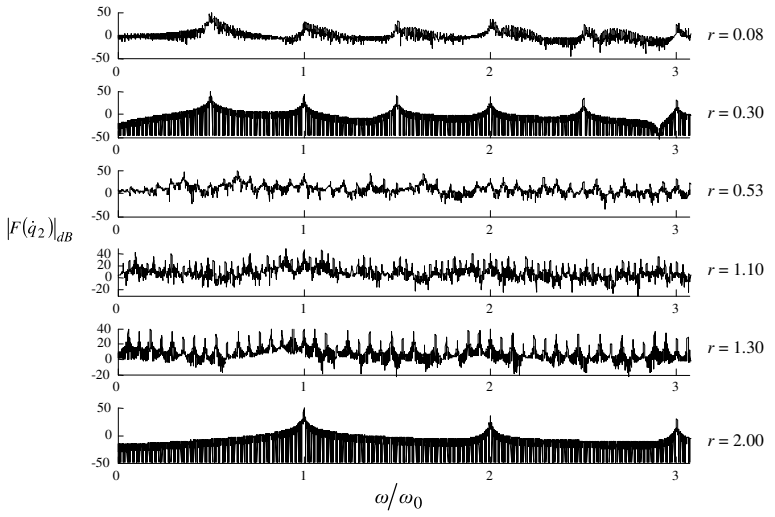

Fig. 8. $|F\{\dot{q}_2(t)\}|$ of the 3R-robot during 300 cycles, versus the frequency ratio ω/ω_0, for $r = \{0.08, 0.30, 0.53, 1.10, 1.30, 2.00\}$, $\rho = 0.7$, $\omega_0 = 7.0$ rad sec^{-1}.

4. Analysis of the robot trajectories

In the previous Section, we verified that the pseudoinverse-based algorithm leads to unpredictable arm configurations. In order to gain further insight into the pseudoinverse nature several distinct experiments are devised in the sequel during a time window of 300 cycles. Therefore, in a first set of experiments, we calculate the Fourier transform of the $3R$-robot joints velocities for a circular repetitive motion with frequency $\omega_0 = 7.0$ rad sec^{-1}, radius $\rho = \{0.1, 0.3, 0.5, 0.7\}$ and radial distances $r \in]0, L_{\mathrm{TOT}} - \rho[$.

Figs. 4–7 show $| F\{\dot{q}_2(t)\} |$ versus the frequency ratio ω_0/ω and the distance r where $F\{\}$ represents the Fourier operator.

Is verified an interesting phenomenon induced by the gripper repetitive motion ω_0 because a large part of the energy is distributed along several sub-harmonics. These fractional-order harmonics (*foh*) depend on r and ρ making a complex pattern with similarities with those revealed by chaotic systems. Furthermore, we observe the existence of several distinct regions depending on r.

For example, selecting in Fig. 7 several distinct cases, namely for $r = \{0.08, 0.30, 0.53, 1.10, 1.30, 2.00\}$, we have the different signal Fourier spectra clearly visible in Fig. 8.

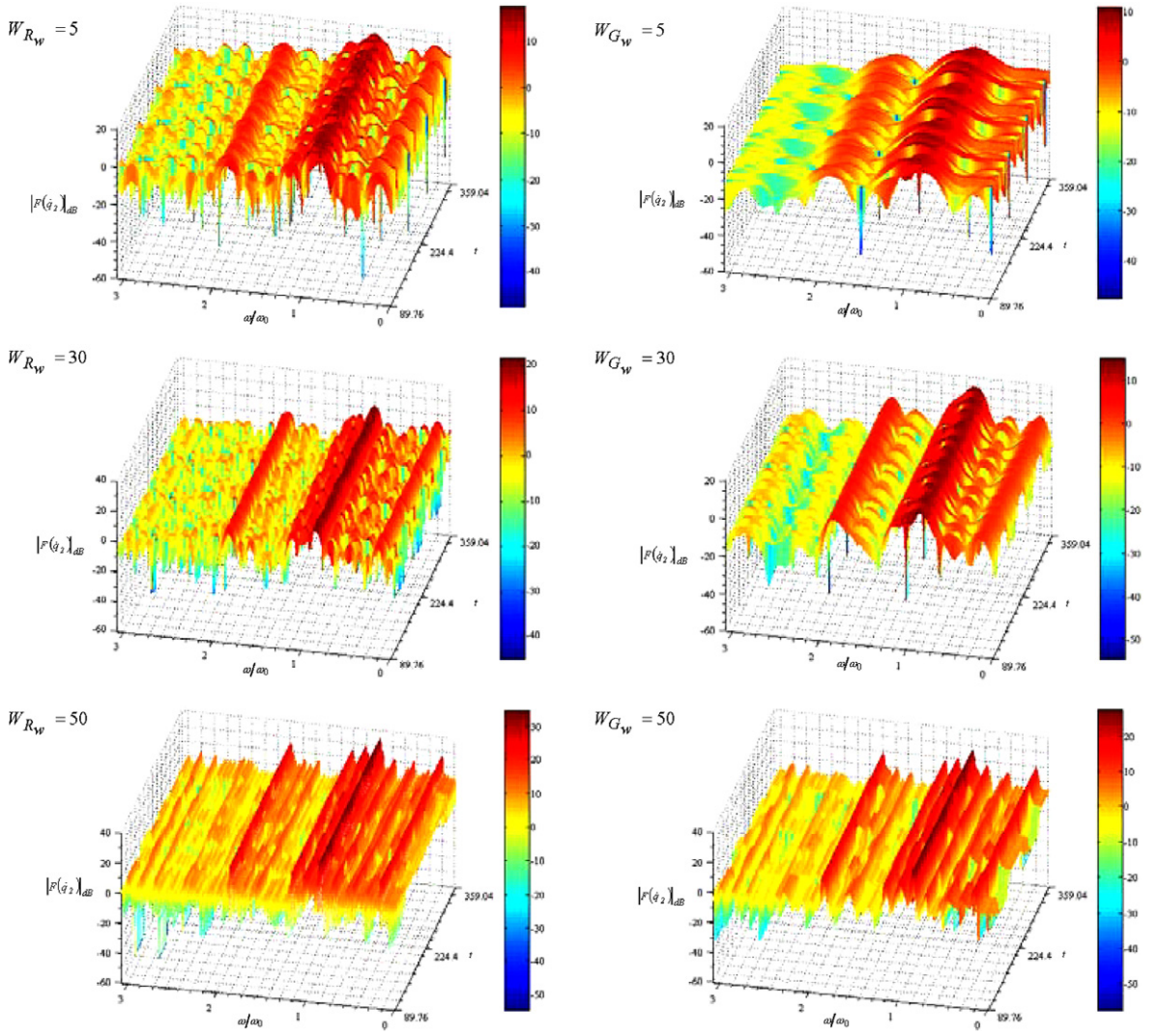

Fig. 9. $| F_{R_w}\{\dot{q}_2(t)\} |$ of the $3R$-robot during 300 cycles, versus $(t, \omega/\omega_0)$, for $\rho = 0.5$, $r = 0.6$, $\omega_0 = 7.0$ rad sec^{-1}, $W_{R_w} = \{5, 30, 50\}$ cycles and $W_{G_w} = \{5, 30, 50\}$ cycles.

To the best knowledge of the authors, the *foh* are aspects of fractional dynamics [14–16], but a final and assertive conclusion about a physical interpretation is a matter still to be explored.

For joints velocities 1 and 3 the results are similar to the verified ones for joint velocity 2.

In order to capture the time evolution of the joint variables, we develop a second set of experiments.

One way of obtaining the time-dependent frequency content of a signal is to take the Fourier transform of a function over an interval around the time instant τ, where τ is a variable parameter [13]. This mathematical tool is called the short-time or windowed Fourier transform (WFT) and may be defined as follows:

$$\{F_{\mathrm{g}}f\}(\omega,\tau)=\int_{-\infty}^{+\infty} f(t)\overline{g(t-\tau)}\mathrm{e}^{-\mathrm{i}t\omega}\mathrm{d}t, \tag{8}$$

where $g(t)$ is the window function and $\tau,\omega\in\Re$. The multiplication by $g(t-\tau)$ localizes the Fourier integral in the neighborhood of $t=\tau$.

The slice of information provided by $\{F_{\mathrm{g}}f\}(\omega,\tau)$ is represented in a time-frequency plane (t,ω) by a region whose location and width depends on the time-frequency spread of $g_{\omega,\tau}(t)=\mathrm{e}^{\mathrm{i}t\omega}g(t-\tau)$. If $\mu(g)$ and $\sigma(g)$ are the centre and the radius, respectively, of the window function $g(t)$, then $\{F_{\mathrm{g}}f\}(\omega,\tau)$ gives information about f

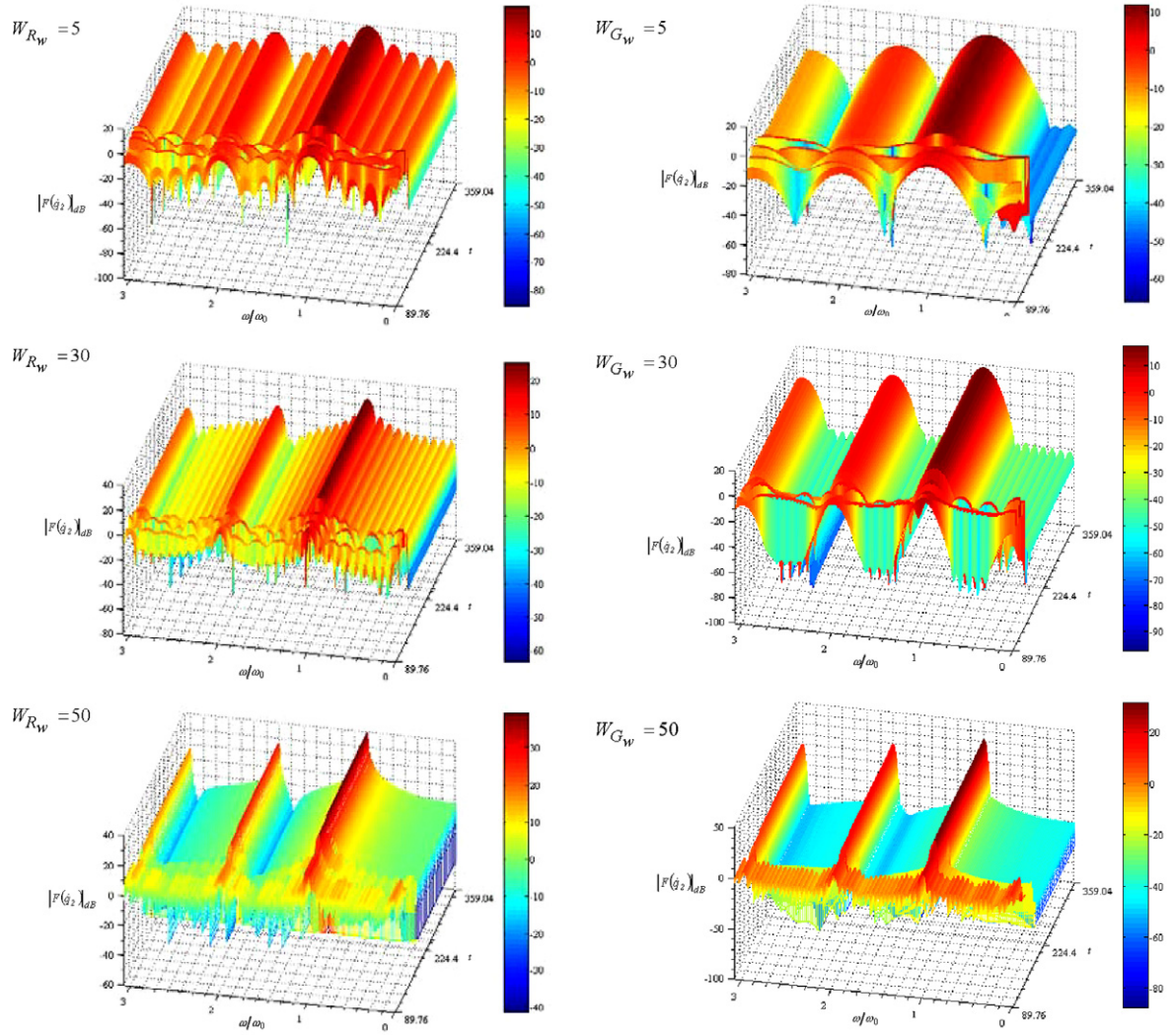

Fig. 10. $|F_{R_w}\{\dot{q}_2(t)\}|$ of the $3R$-robot during 300 cycles, versus $(t,\omega/\omega_0)$, for $\rho=0.5$, $r=1.289$, $\omega_0=7.0$ rad sec^{-1}, $W_{R_w}=\{5,30,50\}$ cycles and $W_{G_w}=\{5,30,50\}$ cycles.

and F, essentially in the region $I_t \times I_\omega$ of the time-frequency plane where $\hat{g} = F(g), I_t \equiv [\mu(g) + \tau - \sigma(g), \mu(g) + \tau + \sigma(g)]$ and $I_\omega \equiv [\mu(\hat{g}) + \omega - \sigma(\hat{g}), \mu(\hat{g}) + \omega + \sigma(\hat{g})]$.

The Heisenberg uncertainty proves that the area of this region is [17]:

$$\sigma(g)\,\sigma(\hat{g}) \geqslant 1/2, \tag{9}$$

and this principle states that precise localizations both, on time and frequency, are mutually exclusive. Thus, this trade-off between temporal and frequency resolution always exists [17,18]. Moreover, the size of this region is independent of (τ, ω), which means that the WFT has the same resolution across the time-frequency plane.

In the experiments, we adopt two window functions, $\Psi := \{R_{\mathrm{w}}, G_{\mathrm{w}}\}$, namely rectangle and Gaussian windows $R_{\mathrm{w}}(t) = 1$, and $G_{\mathrm{w}}(t) = \mathrm{e}^{-at^2/2}, (a = 18), t \in W_\Psi$. Moreover, we choose two that leads to non-overlapping time windows. In the sequel, the corresponding WFTs are represented by $F_{R_{\mathrm{w}}}$ and $F_{G_{\mathrm{w}}}$, respectively.

Figures 9–11 show $|\, F_\Psi\{\dot{q}_2(t)\}\,|$, with window width $W_\Psi = \{5, 30, 50\}$ cycles, $\Psi := \{R_{\mathrm{w}}, G_{\mathrm{w}}\}$, for $\rho = 0.5$ and $r = \{0.6, 1.289, 2.0\}$. We verify [18] that choosing a shorter (larger) time window W_Ψ increases (decreases) the temporal resolution but, on the other hand, decreases (increases) the frequency resolution.

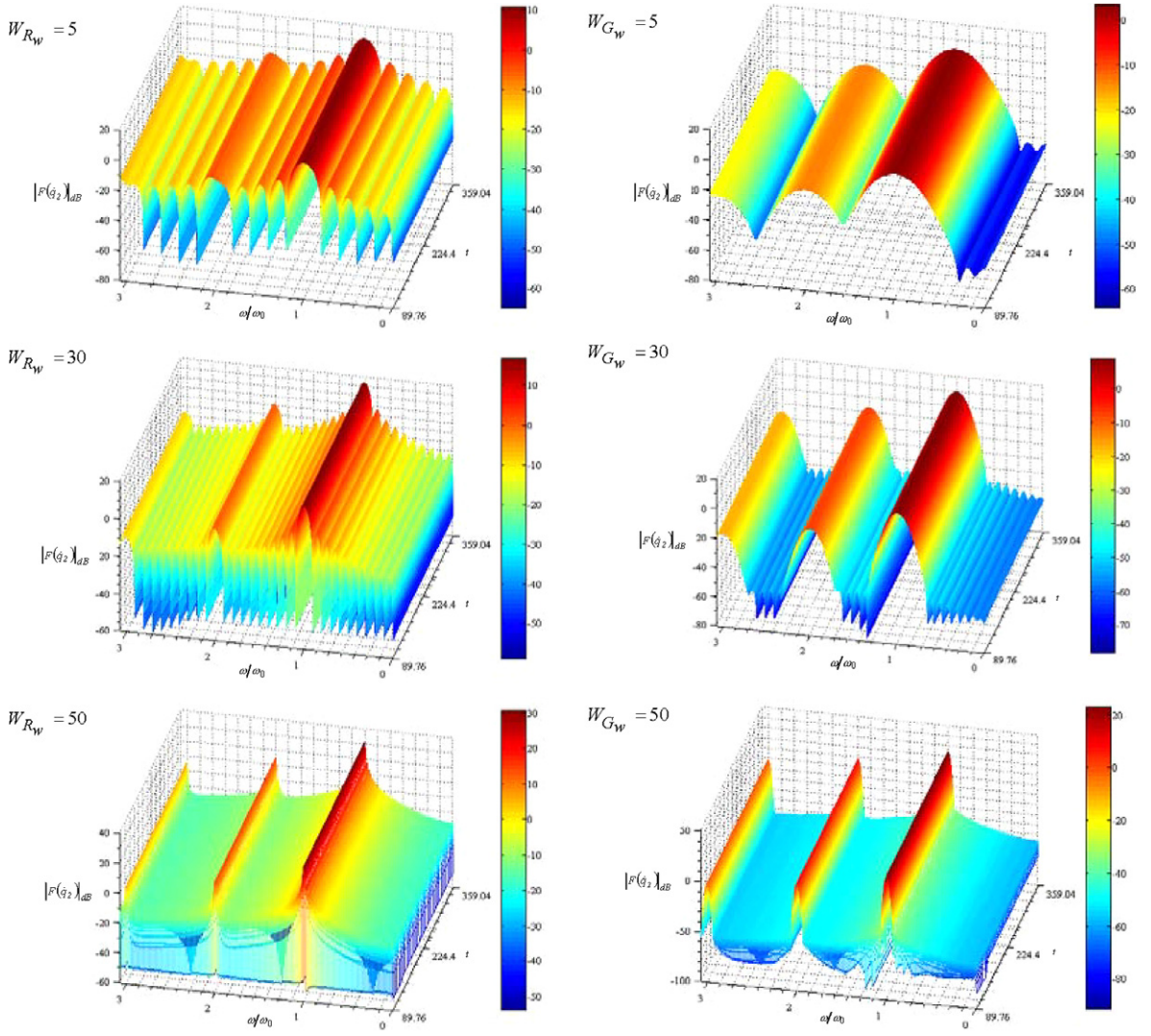

Fig. 11. $|\, F_{R_{\mathrm{w}}}\{\dot{q}_2(t)\}\,|$ of the $3R$-robot during 300 cycles, versus $(t, \omega/\omega_0)$, for $\rho = 0.5$, $r = 2.0$, $\omega_0 = 7.0$ rad sec^{-1}, $W_{R_{\mathrm{w}}} = \{5, 30, 50\}$ cycles and $W_{G_{\mathrm{w}}} = \{5, 30, 50\}$ cycles.

In Fig. 9 ($r = 0.6$), we observe that the distribution of the signal energy dependents on the time evolution.

In fact, the signal energy of the fundamental harmonic oscillates periodically and we verify that a large amount of the signal energy concentrates at several *foh*.

In Fig. 10 ($r = 1.289$), we verify that we have two distinct regions: a first one for the leading 60 cycles and a second for the remaining 240 cycles. In the first region, we have a signal energy distribution along all frequencies, while in the second, the energy is concentrated in the fundamental and multiple higher harmonics.

Finally, in Fig. 11 ($r = 2.0$), we get a regular behavior and the WFTs are invariant with time.

In all figures 9–11, the phenomena occur independently of the shape $\Psi := \{R_w, G_w\}$ or the width W_Ψ of the time window.

5. Conclusions

This paper discussed several aspects of the phenomena generated by the pseudoinverse-based trajectory control of the $3R$ redundant manipulators.

The closed-loop pseudoinverse's method leads to non-optimal responses, both for the manipulability and the repeatability. Bearing these facts in mind the chaotic responses were analyzed from different point of views, namely phase plane and Fourier transform. The results revealed the appearance of radial distances for which a large part of the energy is distributed in fractional-order harmonics. In order to capture the time evolution of the joint variables we develop a set of experiments based on the WFT. The results showed that the frequencies of the joint velocity depend on the time evolution.

References

[1] Sahin Conkur E, Buckingham Rob. Clarifying the definition of redundancy as used in robotics. Robotica 1997;15:583–6.

[2] Chiaverini S. Singularity-robust task-priority redundancy resolution for real time kinematic control of robot manipulators. IEEE Trans Robotic Autom 1997;13:398–410.

[3] Klein CA, Huang CC. Review of pseudoinverse control for use with kinematically redundant manipulators. IEEE Trans Syst Man, Cyber 1983;13:245–50.

[4] Yoshikawa T. Foundations of robotics: analysis and control. MIT Press; 1988.

[5] Rodney Roberts R, Maciejewski Anthony. Singularities, stable surfaces and repeatable behavior of kinematically redundant manipulators. Int J Robotic Res 1994;13:70–81.

[6] Bay John. Geometry and prediction of drift-free trajectories for redundant machines under pseudoinverse control. Int J Robotic Res 1992;11:41–52.

[7] Nakamura Y. Advanced robotics: redundancy and optimization. Addison-Wesley; 1991.

[8] Doty Keith L, Melchiorri C, Bonivento C. A theory of generalized inverses applied to robotics. Int J Robotic Res 1993;12:1–19.

[9] Siciliano Bruno. Kinematic control of redundant robot manipulators: a tutorial. J Intell Robot Syst 1990;3:201–12.

[10] Chung WJ, Youm Y, Chung WK. Inverse kinematics of planar redundant manipulators via virtual links with configuration index. J Robot Syst 1994;11:117–28.

[11] Seereeram Sanjeev, Wen John T. A global approach to path planning for redundant manipulators. IEEE Trans Robotic Autom 1995;11:152–9.

[12] Fernando Duarte JA, Machado Tenreiro. Chaotic phenomena and fractional-order dynamics in the trajectory control of redundant manipulators. Nonlinear Dynamics, vol. 29. USA: Kluwer; 2002. p. 315–42. 1–4.

[13] Mallat Stéphane. A wavelet tour of signal processing. Academic Press; 1999.

[14] Machado JAT. Analysis and design of fractional-order digital control systems. SAMS – J Syst Anal Model Sim 1997;27:107–22.

[15] Machado JAT. Discrete-time fractional-order controllers. FCAA - J Fract Calc Appl Anal 2001;4(1):47–66.

[16] da Graça Marcos Maria, Duarte Fernando BM, Tenreiro Machado JA. Complex dynamics in the trajectory control of redundant manipulators, nonlinear science and complexity. World Scientific; 2007. 134–43.

[17] Ozaktas Haldun M, Zalevsky Zeev, Alper Kutay M. The fractional Fourier transform with applications in optics and signal processing. John Wiley and Sons Ltd.; 2001.

[18] Hubbard Barbara Burke. The world according to wavelets. A K Peters Ltd.; 1998.